Xiaolong Bai
School of Materials Engineering,
Purdue University,
West Lafayette, IN 47907;
Center for Materials Processing and Tribology,
Purdue University,
West Lafayette, IN 47907
e-mail: xlbai725@outlook.com

Andrew B. Kustas
Material, Physical and Chemical Sciences Center,
Sandia National Labs,
Albuquerque, NM 87185
e-mail: akustas@sandia.gov

James B. Mann
M4 Sciences Corporation,
Lafayette, IN 47906
e-mail: jbmann@m4sciences.com

Srinivasan Chandrasekar
Center for Materials Processing and Tribology,
Purdue University,
West Lafayette, IN 47907
e-mail: chandy@purdue.edu

Kevin P. Trumble[1]
School of Materials Engineering,
Purdue University,
West Lafayette, IN 47907;
Center for Materials Processing and Tribology,
Purdue University,
West Lafayette, IN 47907
e-mail: driscol@purdue.edu

Shear-Based Deformation Processing of Age-Hardened Aluminum Alloy for Single-Step Sheet Production

Shear-based deformation processing by hybrid cutting-extrusion and free machining are used to make continuous strip, of thickness up to 1 mm, from low-workability AA6013-T6 in a single deformation step. The intense shear can impose effective strains as large as 2 in the strip without pre-heating of the workpiece. The creation of strip in a single step is facilitated by three factors inherent to the cutting deformation zone: highly confined shear deformation, in situ plastic deformation-induced heating, and high hydrostatic pressure. The hybrid cutting-extrusion, which employs a second die located across from the primary cutting tool to constrain the chip geometry, is found to produce strip with smooth surfaces ($S_a < 0.4$ μm) that is similar to cold-rolled strip. The strips show an elongated grain microstructure that is inclined to the strip surfaces—a shear texture—that is quite different from rolled sheet. This shear texture (inclination) angle is determined by the deformation path. Through control of the deformation parameters such as strain and temperature, a range of microstructures and strengths could be achieved in the strip. When the cutting-based deformation was done at room temperature, without workpiece preheating, the starting T6 material was further strengthened by as much as 30% in a single step. In elevated-temperature cutting-extrusion, dynamic recrystallization was observed, resulting in a refined grain size in the strip. Implications for deformation processing of age-hardenable Al alloys into sheet form, and microstructure control therein, are discussed.
[DOI: 10.1115/1.4052441]

Keywords: age-hardening aluminum alloys, sheet processing, workability, dynamic recrystallization, machining, advanced materials and processing, bulk deformation processes (e.g., extrusion, forging, wire drawing), nontraditional manufacturing processes

1 Introduction

Aluminum alloys, especially those of the age-hardenable 2xxx, 6xxx, and 7xxx series, have long been used in aircraft structural applications, mainly because of their high strength-to-weight ratio. There is now much interest also in the use of these alloys in the automotive sector, driven by similar light-weighting considerations. Consequently, there is a need for efficient processing routes (e.g., cost, process energy) for these alloys to produce them in sheet and foil forms. Work-hardenable 5xxx aluminum alloys have traditionally been used for automotive applications due to their relatively low cost and high formability. But the occurrence of Lüders bands in sheet metal forming processes prevents these alloys from being used in automotive exterior panels where surface finish is important. Serrated deformation in these Al-alloys has therefore been the subject of much study, for instance in notched-bend and tensile testing of Al-Zn-Mg type alloys [1], and tensile testing of rolled and annealed Al 5754 sheet [2,3]. In contrast, heat-treatable 6xxx series aluminum alloys are quite attractive to the automotive sector for body panel applications because of good combination of formability, surface finish, and mechanical properties, see Ref. [4].

Commercial production of Al alloy sheet usually requires many incremental hot- and cold-rolling steps, starting from initial thick cast slabs to the final thin gauge sheet [5]. Total cumulative thickness reductions in reaching sheet forms are typically >99.5%. The majority of this reduction occurs by hot-rolling, which requires the massive starting slab to be heated to high temperatures (~500 °C), with intrinsic large energy costs. The initial hot-rolling (breakdown) is done in a reversing mill, which lengthens the slab to as much as 200 m while it is still too thick to coil. Reversing rolling is then followed by continuous (tandem) hot-rolling, before finishing by cold-rolling. The multistage rolling has advantages for large-scale, continuous production of sheet, but it is quite energy intensive and requires large-scale infrastructure.

Hybrid cutting-extrusion (HCE), a highly confined, simple-shear deformation process involving constrained chip formation by cutting (Fig. 1), has the potential to significantly reduce the number of processing steps required in sheet metal production. It is a single-step process that utilizes constrained plane-strain deformation to produce sheet by chip formation directly from an ingot. A sharp, wedge cutting tool with rake angle (α) removes a layer of material of undeformed chip thickness (t_0) from a workpiece rotating with surface velocity (V_0). The chip—the sheet product—forms by simultaneous cutting and extrusion, with the thickness (t_c) of the sheet removed being determined a priori by the position of a second constraining edge/tool located directly across from the primary cutting tool, see Fig. 1. The constraining edge can be configured

[1]Corresponding author.

Manuscript received April 8, 2021; final manuscript received August 30, 2021; published online October 29, 2021. Assoc. Editor: Steven Schmid.

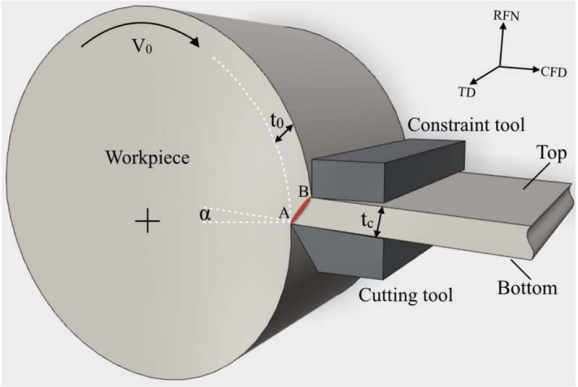

Fig. 1 Schematic of plane-strain hybrid cutting-extrusion (HCE) showing production of sheet by simultaneous cutting and extrusion. CFD, RFN, and TD indicate chip flow, rake face normal and transverse directions, respectively. The top and bottom surfaces of the strip are also labeled.

to achieve different degrees of constraint, as characterized by the chip thickness ratio ($\lambda = t_c/t_0$). In fact, an early version of constrained machining [6] even demonstrated production of wire of circular cross section. HCE differs from free machining (FM) in that this constraining edge is also operating on the chip formation in addition to the primary tool edge. Unlike FM, where $\lambda > 1$ and cannot be controlled a priori, λ in HCE can be set greater or less than 1.

Prior studies have shown that the cutting-extrusion can be used to produce sheet and foil from low-workability alloys like hcp Mg and Ti [7–9] and bcc Fe-Si electrical steels [10], because of certain unique deformation attributes of the process that are favorable for workability. These observations suggested that HCE could potentially be of value for also processing of low-workability, age-hardening Al alloys (e.g., 6XXX series) in sheet form, with interesting combinations of microstructure and texture. In these Al alloys, the workability is severely limited in the aged condition, due to microstructure effects that are quite different from those encountered in the Mg, Ti, and Fe-Si alloys studied earlier. This motivated the present investigation to further explore and analyze the capability of the constrained shear-based deformation processing for producing sheet from low-workability Al alloys.

In the present study, we explore sheet processing of low-workability Al alloys by HCE, using age-hardening 6013-T6 [11] as the model system. The origin of the low workability in this alloy system is fundamentally different from that of the Mg and Ti alloys (limited slip systems and flow localization), and Fe-Si system (compositional (low) workability) studied earlier. Hence, it constitutes an important piece of a research program aimed at understanding production of metal sheet/strip from the spectrum of low-workability alloys by machining-based deformation processing. The strength of 6013 alloy in the T6-aged condition is higher than most other 6xxx aluminum alloys, due to additional Cu and Mg. The tensile strength of the alloy is 405 MPa compared to 310 MPa for the widely used 6061-T6. However, its uniform elongation (ductility) is only 9%, much less than that of the 6061-T6 [12]. Thus, 6013-T6 has intrinsically low workability in conventional deformation processing (e.g., rolling) and, hence, is a suitable model material system for exploration of HCE with (low-workability) age-hardening alloys. It should be noted, however, that in practice, age-hardening aluminum alloys are not normally subjected to significant deformation after developing a significant fraction of their strength during the heat treatment (solution treatment and aging). Production of thin strips of this poor workability alloy, and with good surface quality, is demonstrated. This is accomplished with minimal workpiece preheating and with sheet strains of 1–2. Microstructure development due to the large-strain shear deformation is also characterized. The results, building on related recent work that demonstrated Al flat-wire production by machining-based deformation processing [13], establish the potential of HCE for single-step processing of age-hardening Al alloys of low workability into sheet forms. They also provide a basis for follow-on detailed study of specific deformation attributes and sheet properties.

2 Background

2.1 Mechanics of Hybrid Cutting-Extrusion Deformation. Under plane-strain conditions, the deformation in HCE can be idealized as occurring on a single shear plane (AB) that extends from the primary tool edge to the top surface of the chip/workpiece (constraining edge) as shown in Fig. 1, see Refs. [7,14]. An upper-bound analysis shows that the shear strain (γ) and corresponding von Mises effective strain (ε) in the sheet are [14]

$$\gamma = \sqrt{3}\varepsilon = \frac{\lambda}{\cos\alpha} + \frac{1}{\lambda\cos\alpha} - 2\tan\alpha \tag{1}$$

Effective plastic strains of 1 to 5 can be imposed in a single deformation step by varying λ and α. Note that, unlike rolling, the strain here does not depend on the sheet thickness. Furthermore, such large plastic strains are near-impossible to achieve in sheet rolling due to workability limitations arising from cracking. The large plastic strains result in a high degree of grain refinement and strengthening in the sheet. This high degree of grain refinement and strengthening are also present in other severe plastic deformation (SPD) processes such as equal channel angular pressing, see for example the work on pure Al [15], spray cast Al 7073 [16], and interstitial-free steel [17].

The shear plane orientation and deformation path are controlled by λ and α [18]. This orientation/path determines the crystallographic texture in the sheet. The correlation between deformation path and sheet texture can be predicted from the upper-bound solution, as has been shown in prior work with Mg alloys [7,8], Ti alloys [9], and Fe-Si alloys [10]. All of these alloys are also characterized by poor workability. The prior work demonstrated that a range of shear textures can be obtained in the sheet by varying the deformation path, concurrent with the strengthening by grain refinement. Shear textures are difficult if not impossible to achieve in rolled sheet; see for example the simulations for through-thickness texture gradients in fcc and bcc metals [19], and experimental studies on texture gradients in cold-rolled AA1050 [20] and in commercial purity Al and Cu [21]. Nevertheless, shear textures are attractive for they can enhance formability in sheet metals.

Additional deformation-related attributes of the HCE that are favorable for sheet processing include large hydrostatic pressure [7] and deformation-induced (adiabatic) heating [22] in the shear zone AB due to its highly localized nature (Fig. 1). Both of these process attributes can enhance material workability locally [23,24], thereby reducing or eliminating the need for using workpiece preheating. The deformation zone temperature rise due to adiabatic heating depends on the alloy flow stress and strain rate (directly proportional to V_0) and can usually be estimated from cutting force measurements.

Besides control of deformation parameters (strain, strain rate, and temperature), the single-step HCE is intrinsically more energy efficient than the multi-stage rolling for sheet production because the frictional dissipation is confined to one deformation processing step.

2.2 Suppression of Flow Localization. Cutting-extrusion has also been found suitable to produce sheet from alloys, wherein workability limitations arise primarily from flow localization phenomena like segmentation (e.g., Mg) and/or shear banding (Ti, Fe-Si alloys). Figure 2 shows three examples of this capability for sheet and foil processing in Mg, Ti, and Fe-Si alloys. In hcp magnesium alloy AZ31B, which has limited slip systems active at

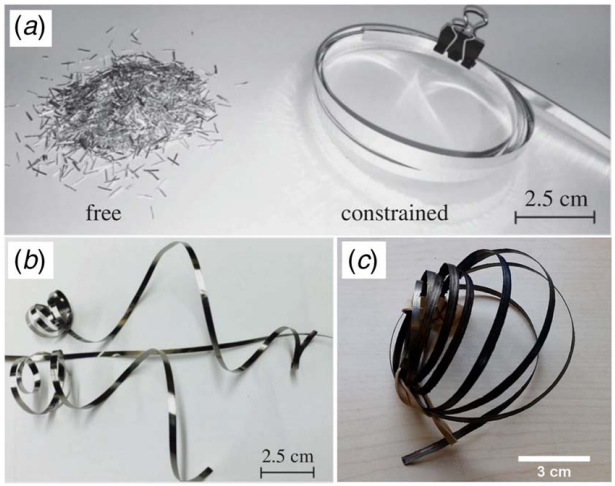

Fig. 2 Capability of HCE to suppress segmentation and shear banding instabilities and produce sheet materials from low-workability alloys. (*a*) Magnesium alloy AZ31B: the left side shows discontinuous chip particles, due to segmentation, in free machining (FM), while the right side shows continuous strip produced by HCE, wherein the segmentation instability has been suppressed; Continuous strip from (*b*) Ti-6Al-4V and (*c*) 4% silicon-iron alloys produced by HCE, wherein shear band instabilities typically giving rise to a saw-tooth chip have been suppressed.

room temperature, HCE has enabled continuous thin strips to be produced without preheating of the workpiece [8]. Without application of the constraint (free machining), the chips produced in this alloy are often in the form of small (discontinuous) particles (Fig. 2(*a*), left) rather than continuous strip. This is because, absent the constraint, the deformation in chip formation is interrupted by fracture leading to the segmented chips. In Mg and Ti [8,9,25] and Fe-Si alloys [10], the constraint can suppress both the shear banding and segmentation instabilities, which constitute a workability barrier for sheet production. Figures 2(*a*) (right) and 2(*b*) show examples of suppression of segmentation and shear band instabilities, respectively, in MgAZ31B and Ti-6Al-4V, achieved using the constraint via HCE. Furthermore, with only modest workpiece preheating and control of strain rate, dynamic recrystallization could also be achieved in the deformation zone in many of these alloys, enabling sheet with homogeneous, fine grain sizes (1–10 μm) to be created. The resulting sheet formability was found to be much better than that of rolled sheet due to favorable shear textures. In high-silicon electrical steels (Fe-Si), which are traditionally produced in sheet form by hot-rolling, due to their high strength and susceptibility to flow localization, the HCE has been successful in effecting sheet/foil production in a single step with only modest or even no workpiece preheating [10]. An example of this is shown in Fig. 2(*c*) with Fe-4% Si alloy, an alloy of very low workability. As with the Mg-AZ31B, a range of fine-grained microstructures and shear textures could be achieved in the Fe-Si steels through control of the deformation conditions.

These observations with Mg, Ti, and Fe-Si alloys provide a basis for experiment design with the age-hardening aluminum alloys.

3 Experimental Procedure

Disk workpieces (150 mm diameter × 7 mm thickness) were cut from commercial rolled AA6013-T6 plate of 14 mm thickness. The chemical composition of this alloy per ASTM B211 is (in wt%): 0.6–1.0 Si, 0.5 Fe, 0.6–1.1 Cu, 0.2–0.8 Mn, 0.8–1.2 Mg, 0.1 Cr, 0.25 Zn, 0.1 Ti, 0.15 others. The through-thickness microstructure of the initial plate (Fig. 3(*a*)) consisted of distinct fine-grained zones with equiaxed grain structure near the surfaces (Fig. 3(*b*)) and a coarse-grained zone with elongated grain structure in the middle (Fig. 3(*c*)). The average grain size in the fine-grained zone was ~40 μm, whereas in the coarse-grain zone, the grains were ~250 μm in the rolling direction (RD) and ~120 μm in the normal direction (ND), as measured by the mean intercept method. This characteristic structure is a remnant of the inhomogeneous deformation occurring in the multi-stage rolling process used to produce the plate. Hardness measurements showed little difference between the fine-grained (137 HV kg/mm^2) and coarse-grained (135 HV kg/mm^2) regions, consistent with the dominant strengthening mechanism being age-hardening. One half of the thickness of the plate was machined off before the disk-shaped workpiece was cut out. Since the strip produced from the edge of this disk by HCE is from both the coarse- and fine-grained regions (Fig. 3(*a*)), the experiment allowed for the response of the fine- and coarse-grained starting material to be studied under identical process conditions in a single specimen/experiment.

A ~7 mm wide cylindrical disk workpiece was mounted on a mandrel in a CNC lathe. The cutting-extrusion tool was fed perpendicular to the disk surface at a specified feed rate per revolution of the disk (see Fig. 1.) The undeformed chip thickness (t_0) was 0.25 mm. High-speed steel cutting tools were used. The initial experiments were conducted without a constraining tool, and these experiments are referred to as FM. The λ ($=t_c/t_0$) value obtained in FM can be termed the natural λ (unconstrained), and it represents the largest strip thickness that can be obtained for a given inlet t_0.

The relative positions of the cutting tool and constraint tool are depicted in Fig. 1. The edge of the constraint tool can be positioned at different heights from the edge of the cutting tool to create the extrusion gap and impose a prescribed chip ratio (λ). The FM strip is used to establish the maximum λ, and, by extension, the maximum extrusion gap between the two tools for the HCE. In the experimental set-up, the extrusion gap is adjusted by placing a hardened steel gage block between the two tool edges, thus prescribing the thickness of the HCE strip. The tool holders are then clamped into position with the gage block in place, and then the block is removed. The edge of the constraint tool is typically offset a small distance, to the right in Fig. 1, relative to the edge of the cutting tool. For the results discussed in the present work, this offset was set 0.025 mm greater than the machining feed rate t_0 (also set using the gage block). The constraint tool is positioned with its "rake face" parallel to the cutting velocity direction in Fig. 1. The constraint tool rake angle was not varied in the experiments.

The HCE experiments were conducted at ambient temperature ($T_0 = 25$°C), with $\alpha = 5$ deg, and $V_0 = 0.5$ and 3 m/s, and two constraint levels, $\lambda = 1.5$ and 0.8. Additional HCE experiments were conducted at elevated (initial) workpiece ambient temperature T_0. In these experiments, the workpiece was preheated in a furnace to 550 °C for 1 h, and then immediately mounted onto the lathe and cutting performed with $t_0 = 0.13$ mm, $\lambda = 1.5$, and $V_0 = 3$ m/s. The ambient temperature of the workpiece during the cutting was $T_0 =$ 400, 300, and 135 °C as recorded by a surface thermocouple. The initial workpiece state for these experiments is thus a solution-treated condition.

The von Mises effective strain (ε) imposed in the strips was estimated from measurement of t_c and t_0, and Eq. (1). This strain was typically ~1 in the HCE and in the range of 2–3.5 for the FM. Some of the strips produced at $T_0 = 25$ °C were annealed at 572 °C for 1 and 4 min and then quenched to room temperature; their properties and microstructure were then compared with those of the strips produced at the higher temperature, but with the same effective strain.

Strip samples for metallographic characterization were prepared by mechanical grinding with 320 to 2000 grit silicon carbide papers, followed by polishing with colloidal silica, and etching with 10 wt% sodium hydroxide for 4–6 min. The through-thickness strip microstructure was investigated by optical

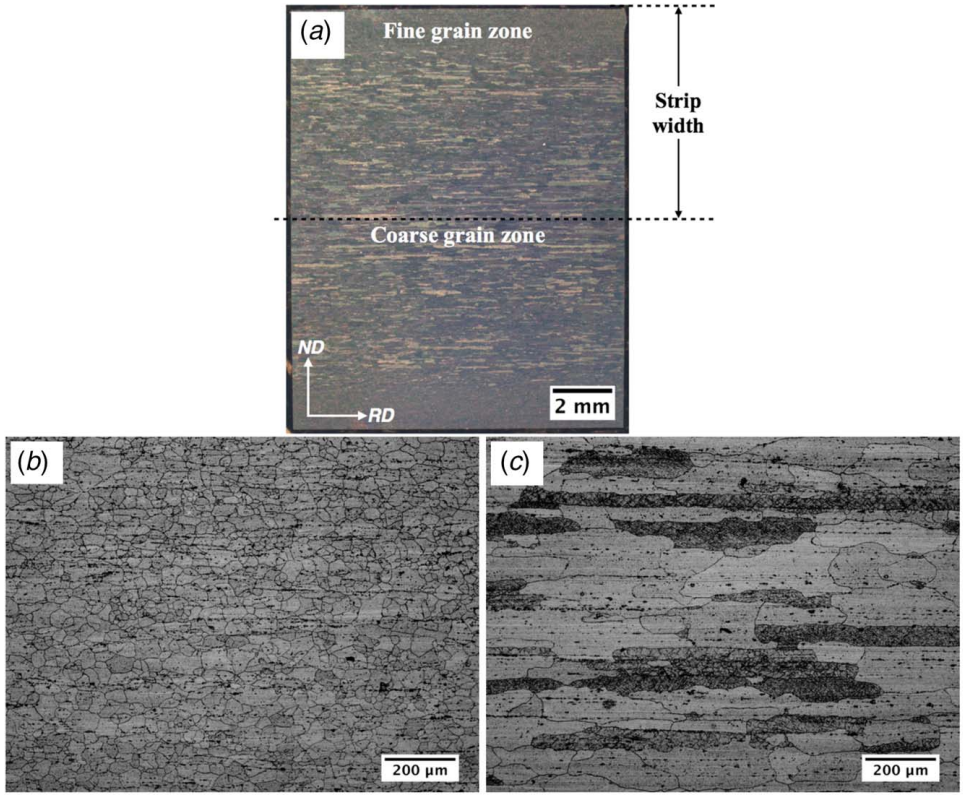

Fig. 3 Microstructure of polished and etched cross sections of (*a*) as-received 6013-T6 plate showing (*b*) fine-grain structure near surfaces and (*c*) coarse-grain structure in the middle. One half of the plate thickness is removed to produce workpieces containing adjacent fine- and coarse-grained regions as indicated in (*a*).

microscopy. Grain size was measured using the mean intercept method by sampling at least 200 distinct grains. Microhardness of the bulk workpiece and strip specimens was measured by Vickers indentation (100-g load) in the central regions of the samples. At least 10 indentations were made in each sample (or location) to obtain an average value for the hardness and related statistics. The typical standard deviation on the hardness value was 3–5%. Surface quality of the sheet produced was characterized by optical profilometry (Zygo NewView 8000) and optical microscopy.

4 Results

4.1 Free Machining at $T_0 = 25$ °C. The FM strips showed significant strain hardening (~25%) relative to the initial T6 (hardness 136 HV) condition of the workpiece. The strips produced at $V_0 = 0.5$ and 3 m/s had average hardness values of 176 and 161 HV, respectively (Table 1). There was negligible difference in the hardness of the strip produced from the fine- and coarse-grain sides of the plate, which is consistent with the dominance of strengthening by age- and strain-hardening. With increasing V_0, the (natural) λ and, hence, effective strain, decreased. But the deformation temperature can be expected to increase with speed due to more adiabatic heating [7]. Both of these effects are consistent with the lower hardness obtained at the higher V_0.

The through-thickness microstructure in the FM strip resulting from the fine- and coarse-grain sides of the initial plate workpiece are shown in Fig. 4. The second phase particles (black) and grain structure provide clear intrinsic markers that capture the shear flow. From the orientation of the flow lines, it is evident that the primary shear deformation in the shear zone is imposed at some

Table 1 Experimental parameters and strain and hardness results

	T_0 (°C)	α (deg)	t_0 (mm)	V_0 (m/s)	t_c (mm)	λ	ε	HV[a] (kgf/mm^2)
AA6013-T6 workpiece								136
FM strip	25	5	0.25	0.5	0.80	3.2	1.9	176
				3	0.52	2.1	1.4	161
HCE strip	25	5	0.25	0.5	0.38	1.5	1.2	138
				3				105
		5	0.25	0.5	0.2	0.8	1.1	155
				3				117
	400	5	0.13	3	0.2	1.5	1.2	89
	300							74
	135							66

[a]The standard deviation on hardness was typically 3–5%.

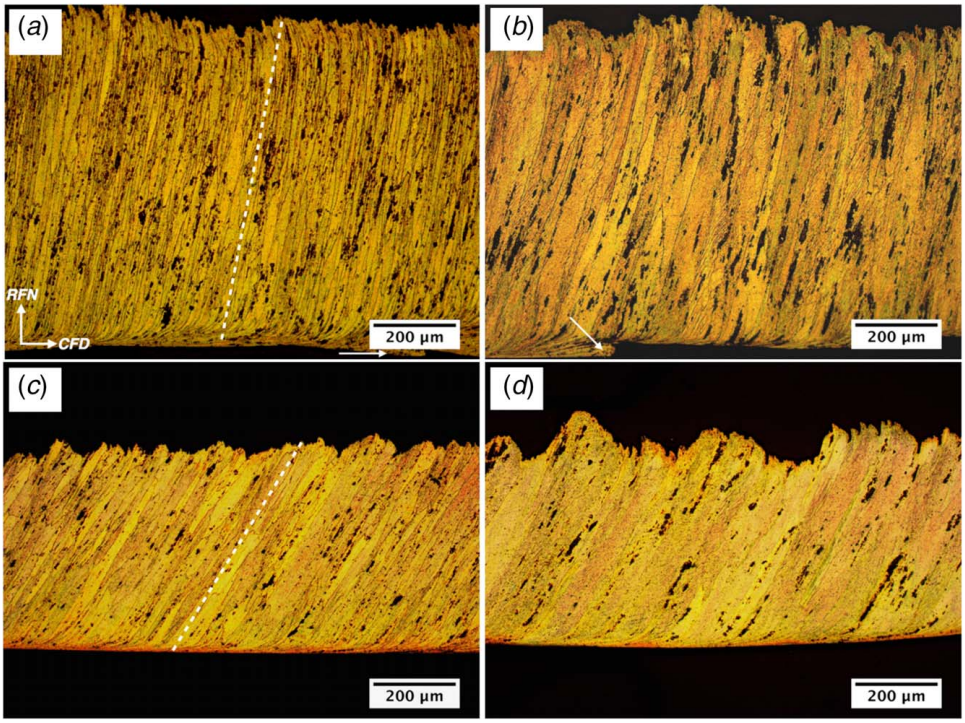

Fig. 4 Through-thickness microstructure of FM Al-alloy strip: (*a*) fine-grain and (*b*) coarse-grain side at $V_0 = 0.5$ m/s, (*c*) fine-grain and (*d*) coarse-grain side at $V_0 = 3$ m/s.

large angle to the strip surface. The flow lines (see, for example, the superimposed white dotted lines in Fig. 4) are the directions of maximum grain elongation, while the shear plane itself represents the direction of maximum shear and is inclined at an angle relative to these flow lines. The angle (φ) between the flow lines and the shear plane is related to the imposed deformation, with the shear strain being $2\cot(2\varphi)$, see Refs. [26,27]. The inclination angle of grains/flow lines to the sheet bottom surface at $V_0 = 0.5$ m/s is ~90 deg and is larger than that at 3 m/s, ~60 deg. This is consistent with a higher level of deformation in the former case. Note that the occurrence of the inclined flow lines is also indicative of a shear texture [8,27].

A very thin secondary shear zone arising from friction at the rake face of the cutting tool is also visible in the images, see along bottom strip surfaces in Fig. 4. In this secondary deformation zone, the flow lines are aligned nearly parallel to the strip (chip) flow direction. This flow zone then makes a sharp transition to the primary shear flow lines. The strip face in contact with the tool is seen to be generally devoid of any built-up edge (BUE), except for the case of low-speed cutting at 0.5 m/s. In this latter case, intermittent remnants of a BUE can be seen along the strip surface, as at white arrows in Figs. 4(*a*) and 4(*b*). In contrast to this flow pattern, rolled-sheet microstructure is characterized by the second phase particles and grains distributed preferentially along the rolling direction (Figs. 3(*b*) and 3(*c*)). This type of flow is analogous to the flow pattern in the secondary deformation zone of the FM strips. Figure 4 also shows that the highly elongated grains originating from the fine-grain zone in the starting material are thinner than those originating from the coarse-grain zone—a direct consequence of the differing starting grain sizes of the material. Although the thickness of the strips was consistent from edge to edge, the course-grained starting material showed increased variability in surface roughness and local thickness across the width of the FM strips (indicated by the more jagged surfaces on the coarse-grained material in Fig. 4). This roughness and thicker deformed grains were more pronounced with increased cutting velocity and the related temperature increase in the cutting zone. Future work will further explore the quantitative effects of the initial grain size and the role of the velocity on the deformed microstructures/textures and dimensional attributes in both the FM and the HCE strips.

It can also be seen from Fig. 4 that the unconstrained (top) surface of the FM strip shows a roughness that is characteristic of the plastic deformation and flow state, whereas the bottom surface (rake face side) is comparatively smooth with its roughness determined by the tool rake face condition. This follows the general result observed in chips produced by machining. A more detailed quantitative analysis of the surfaces is given in Sec. 4.3. Typically, the bottom surface is a close replica of the tool rake surface and hence the small surface roughness on this face. The top surface roughness arises from the lack of confinement of the flow during the FM. This flow, while homogeneous on the macro and meso length scales, is quite non-uniform at the grain-level length scale. Hence, it can be expected to scale with the starting grain size in FM, with the roughness being greater for the strip created from the coarser-grained material. This difference is seen upon comparing Figs. 4(*a*) and 4(*c*) with Figs. 4(*b*) and 4(*d*). Since the starting material has similar hardness in the fine- and coarse-grained

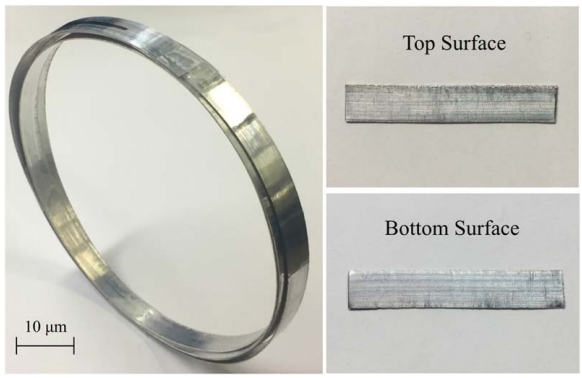

Fig. 5 Continuous HCE Al-alloy strip produced at $V_0 = 3$ m/s, $\lambda = 1.5$, showing smooth top and bottom surfaces

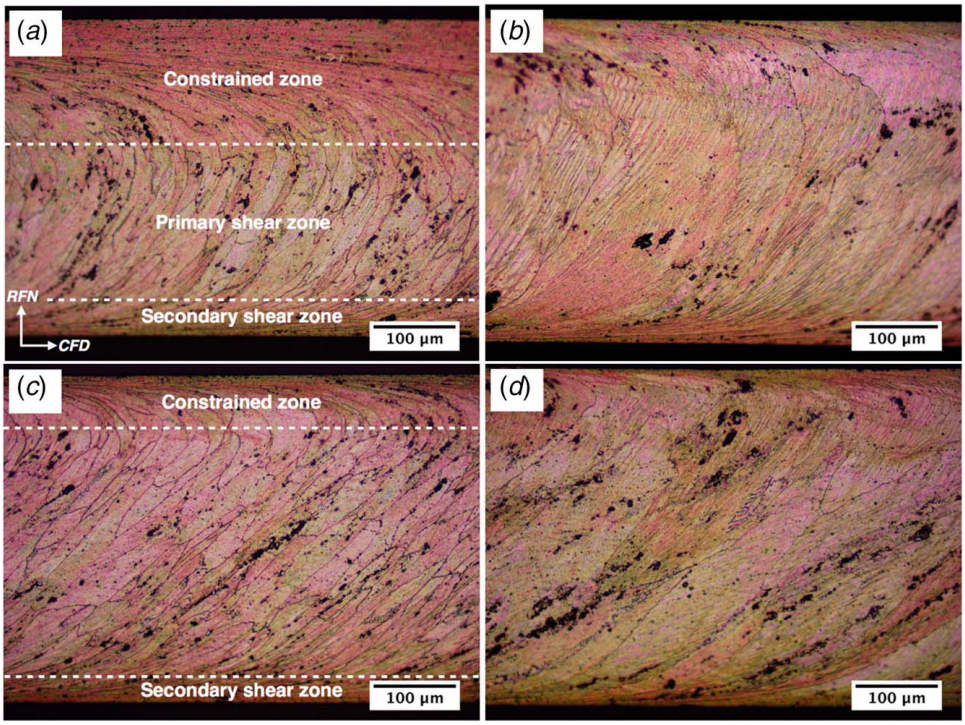

Fig. 6 Through-thickness microstructure of HCE strips at $\lambda = 1.5$: (*a*) fine-grain and (*b*) coarse-grain side at $V_0 = 0.5$ m/s, and (*c*) fine-grain and (*d*) coarse-grain side at $V_0 = 3$ m/s

regions, and both of these regions are exposed to identical processing (deformation) conditions in the strip making, the initial grain size difference is the most probable reason for the observed difference in surface roughness.

4.2 Hybrid Cutting-Extrusion at $T_0 = 25$ °C. Continuous strip produced by HCE at $\lambda = 1.5$, and at the same velocity as in FM, is shown in Fig. 5. Unlike the FM strips, both surfaces of the HCE strips are smooth because of the constraining tool contact along the top surface of the strip (Fig. 5). The application of the constraint removes any microstructure effect on roughness along the strip surfaces. This is in contrast to FM, where the top surface roughness approximately scales with the grain size (Fig. 4). The strips produced by FM and HCE both exhibit some degree of curvature (see Fig. 2). This curvature is influenced by diameter of the disk workpiece, with larger diameter workpieces reducing the strip curvature and relatively smaller diameter workpieces tending to increase it. The specific causes of the curvature and residual stress state of the strip are under investigation.

Figure 6 shows the through-thickness microstructure of the HCE strips. The grain size difference in the two sides of the (starting) disk workpiece is again reflected in the strip microstructure. As in the case of FM, the hardness differences between the fine- and coarse-grain regions in the HCE strip were negligible due to the dominance of the other strengthening mechanisms. However, the hardness of strips produced at 0.5 and 3 m/s, 138 HV, and 105 HV, respectively, was much smaller than the hardness of the strips produced by FM at the same velocities, 176 HV and 161 HV. This difference is due to the greater strain imposed by the FM (Table 1). The deformation shear strains occurring in the primary and secondary shear zone together contribute to the increased hardness of the strip in HCE of strain-hardening alloys.

In the HCE, the constraint confines the flow of the material and acts as an extrusion die concurrent with the cutting tool action. The friction between the constraint and top surface of the strip leads to the formation of another friction-induced shear zone along this contact (Fig. 6) analogous to that along the rake face of the cutting tool (see also Fig. 4). The former region is henceforth referred to as the "constrained zone," while the shear zone along the tool rake face is referred to as the "secondary shear zone" (Fig. 6). At lower V_0, the friction is typically larger; hence, both the constrained zone and secondary shear zones are wider. With increasing velocity and reducing friction, the extent of both the constrained and secondary shear zones decreases and more of the primary shear zone flow pattern is now retained, as seen in Figs. 6(*c*) and 6(*d*). Furthermore, the built-up edge phenomenon is avoided in the constrained cutting even at 0.5 m/s, whereas the built-up edge is seen in FM at this lower velocity.

The microstructure in the strip at $\lambda = 0.8$ (Fig. 7) is quite different from that at $\lambda = 1.5$. Although the effective strain is approximately the same at both these conditions (Table 1), the hydrostatic pressure at $\lambda = 0.8$ is about 1.5 times larger than that at $\lambda = 1.5$ [7]. This increased pressure likely increases the friction between the constraint and strip, leading to the reduction, and even suppression, of the primary shear zone (Fig. 7(*a*)). At $\lambda = 0.8$, the thickness of the constrained zone is larger for the lower V_0. On the other hand, with increasing hydrostatic pressure, the thickness of the grains in the primary shear zone decreases (Figs. 6 and 7), and there is no discernable difference between the microstructure of the strip created from the fine- and coarse-grained regions of the initial workpiece.

The hardness of the strips produced at $\lambda = 0.8$ is modestly higher than those created at $\lambda = 1.5$ for each velocity (Table 1). For each λ, the hardness of the strip decreases with increasing V_0, due most likely to an increased deformation temperature. This increase in temperature with cutting speed, as indicated by the lower hardness, however, is still not sufficient enough for any dynamic recrystallization to occur in the strip (Fig. 7).

4.3 Surface Roughness. Figure 8 shows optical profilometer images of surfaces of FM strip at $V_0 = 3$ m/s (corresponding to Figs. 4(*c*) and 4(*d*)) and of HCE strip at the same V_0 ($\lambda = 1.5$) (corresponding to Figs. 6(*c*) and 6(*d*)). The bottom surface of FM strip is quite smooth with $S_a = 0.37$ μm (Fig. 8(*b*)), significantly smoother than the top surface, for which the roughness is $S_a =$

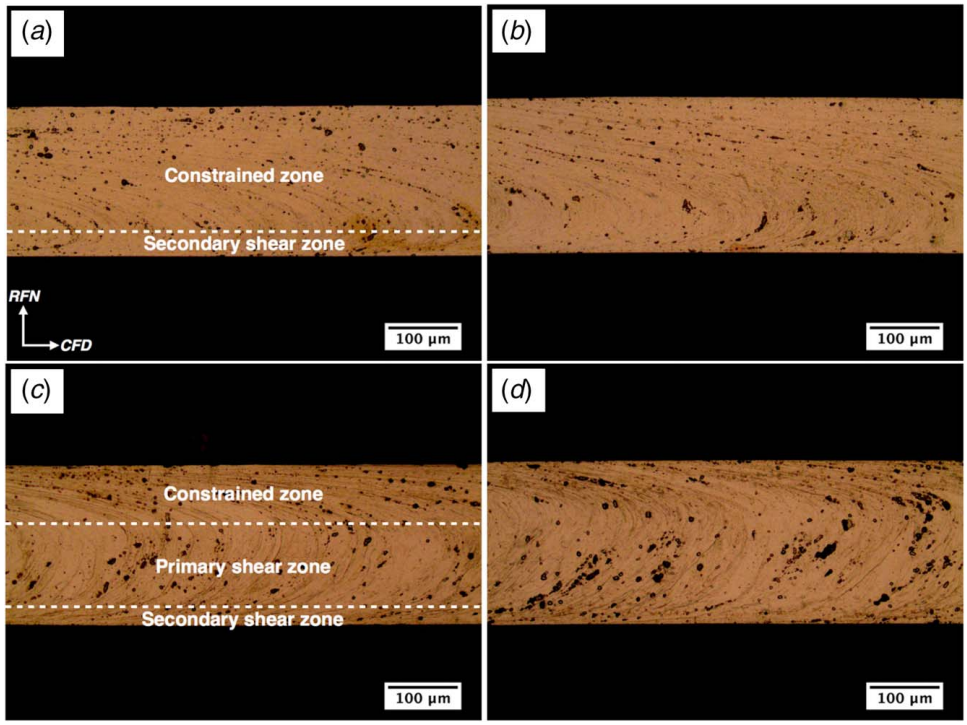

Fig. 7 Through-thickness microstructure of HCE strips at $\lambda = 0.8$: (*a*) fine-grain and (*b*) coarse-grain side at $V_0 = 0.5$ m/s, (*c*) fine-grain and (*d*) coarse-grain side at $V_0 = 3$ m/s.

20.76 μm (Fig. 8(*a*)). For the HCE strip, however, the surface quality of the top and bottom surface is similar, with $S_a =$ 0.36 μm (Fig. 8(*d*)) for the bottom surface and $S_a = 0.43$ μm for the top surface (Fig. 8(*c*)). A 50-fold reduction in surface roughness on the top surface is achieved by HCE. Hence, the constraint improves the surface quality quite effectively, making the top and bottom surfaces essentially identical. For comparison, the surface roughness on commercial rolled sheet surfaces is typically ~0.4 μm [28].

4.4 Hybrid Cutting-Extrusion at Elevated Temperature. The results from HCE experiments conducted at elevated temperatures (preheating the workpiece) are summarized in Table 1. The

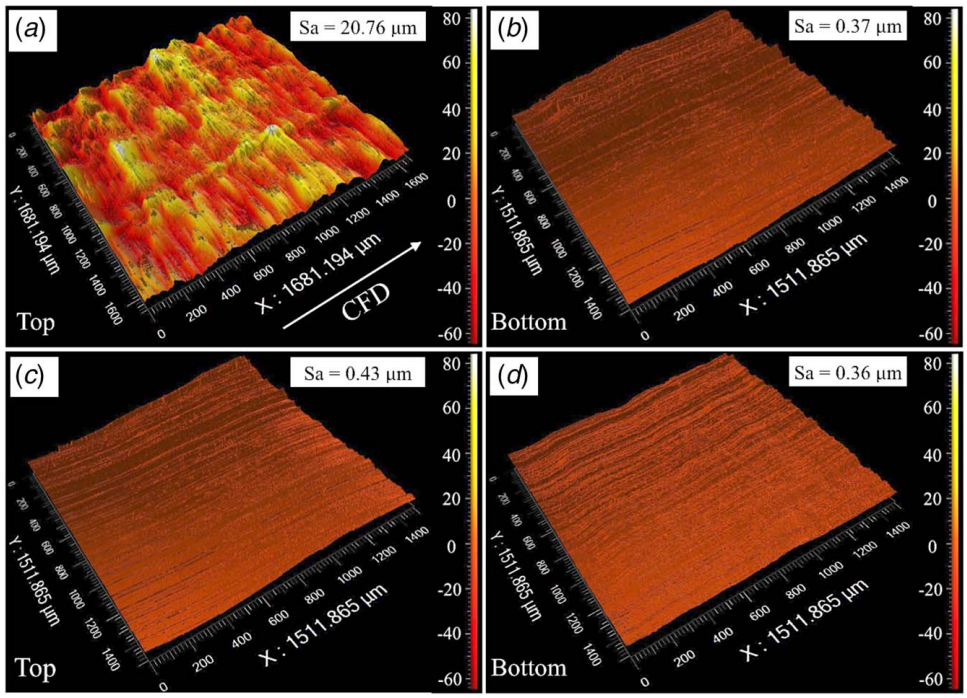

Fig. 8 Optical profilometry images of surface topography of (*a*) top and (*b*) bottom surface of FM strip at $V_0 = 3$ m/s, $t_0 = 0.25$ mm, (*c*) top and (*d*) bottom surface of HCE strip at $V_0 = 3$ m/s, $t_0 =$ 0.25 mm, and $\lambda = 1.5$

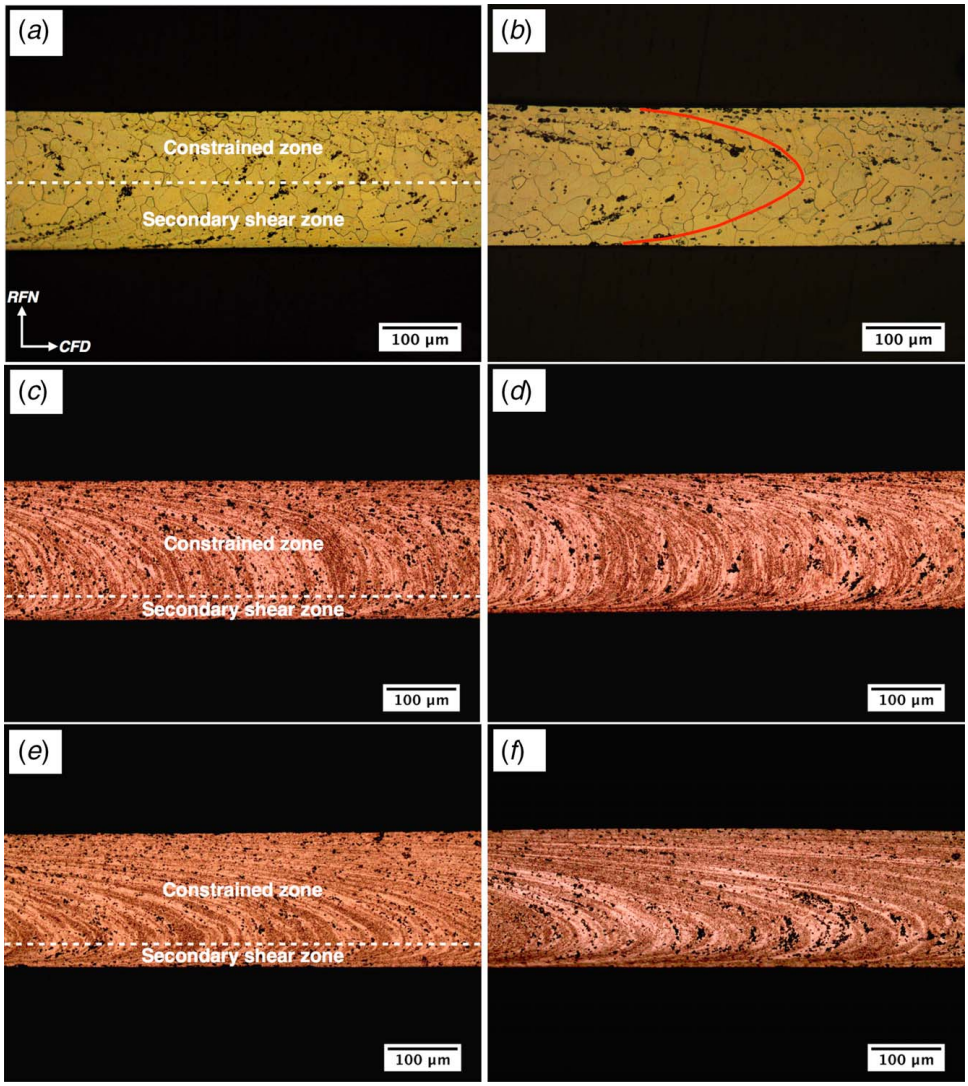

Fig. 9 Through-thickness microstructure of HCE strips at $\lambda = 1.5$: (*a*) fine-grain and (*b*) coarse-grain side at $T_0 = 400$ °C showing dynamically recrystallized microstructure, (*c*) fine-grain and (*d*) coarse-grain side at $T_0 = 300$ °C, (*e*) fine-grain and (*f*) coarse-grain side at $T_0 = 135$ °C. The line in (*b*) outlines the shear flow pattern.

strip hardness values are all significantly lower than in the corresponding room-temperature experiments; these hardness values (65–90 HV) are, in fact, in the hardness range for the alloy in an annealed condition. The corresponding through-thickness microstructures are shown in Fig. 9. For $T_0 = 400$ °C, complete dynamic recrystallization is observed (Figs. 9(*a*) and 9(*b*)). The grain size (21 μm) is much refined compared with that in the initial workpiece (~40 μm on surface and ~120 μm in the middle, Figs. 3(*b*) and 3(*c*)); note that this refinement is achieved in just a single step of deformation. Furthermore, through-thickness microstructures along both sides of the strip are quite homogeneous (Figs. 9(*a*) and 9(*b*)). Both of these structures have the same grain size (around 20 μm) despite the much different, initial workpiece microstructure (Figs. 3(*b*) and 3(*c*)). Thus, the initial grain size in the workpiece does not affect the dynamically recrystallized microstructure, since the latter is likely determined only by the imposed strain and temperature.

The microstructures of strips produced at the lower T_0 of 300 °C (Figs. 9(*c*) and 9(*d*)) are quite different from those at $T_0 = 400$ °C (Figs. 9(*a*) and 9(*b*)). Dynamic recrystallization is now suppressed due to the lower deformation zone temperature. A flow-line type microstructure, with grains unresolved, is observed, similar to that of strips produced at room temperature (Figs. 6 and 7). Figures 9(*e*) and 9(*f*) show the microstructures of HCE strips produced at even lower $T_0 = 135$ °C. A highly deformed, flow-line type microstructure, akin to that at $T_0 = 300$ °C, is again obtained.

4.5 Static Recrystallization. To validate the dynamic recrystallization occurring in situ in HCE, a few static recrystallization experiments were carried out. Strips produced at room temperature with $\lambda = 1.5$ and $V_0 = 3$ m/s (Table 1 and Figs. 6(*c*) and 6(*d*)) were annealed at ~570 °C for 1 to 4 min and then water quenched to simulate a continuous annealing process. After the 1-min anneal, the strips were found to be completely recrystallized with a homogeneous microstructure on both sides of the strip (Figs. 10(*a*) and 10(*b*)). This microstructure is similar to that observed in the HCE strip at $T_0 = 400$ °C; for example, the average grain size in the statically annealed strip, 20 μm, was essentially the same as that in the dynamically recrystallized strip, 21 μm. Upon increasing the annealing time to 4 min, there was no distinguishable change in the microstructure. The hardness values of the statically recrystallized strips (93 HV) were only slightly larger than those of the HCE strips that had dynamically recrystallized (89 HV). These static recrystallization observations reinforce the conclusion that dynamic recrystallization had indeed occurred in the HCE with the workpiece

pre-heated at the high temperature condition. And, they also support the viability of using short-time, continuous annealing of HCE strips, wherever produced without workpiece preheating, to obtain sheet with recrystallized microstructures analogous to conventional commercial practice (cold rolling + heat treatment).

5 Discussion

The experiments have shown that shear-based deformation processing by HCE can be used to produce metal strip from high-strength, age-hardened Al alloy 6013-T6. This extends prior work with low-workability Mg, Ti, and Fe-Si alloys to another model low-workability system, wherein the poor workability is due to microstructure effects. Production of continuous strip, directly from the AA6013-T6 (age-hardened), in a single step even without workpiece preheating, has been demonstrated. The microstructures range from severely cold-worked to dynamically recrystallized with fine, homogeneous, equiaxed grain structure. The strip texture is likely a shear texture, as indicated by the inclination of the flow lines in the strip, see Refs. [7,8]. Furthermore, compared with conventional rolling, the HCE offers better control of deformation parameters such as strain, strain rate, and temperature. The results have implications for economic production of sheet, with controlled microstructure and properties.

The HCE process is configured around plane-strain machining. Dimensional scaling to produce sheet of commercial width and thickness is limited only by the power capacity of the machine configuration and not by any deformation process mechanics. In the present study, small-scale strip ~7 mm wide was produced on a CNC lathe setup to investigate effects related to deformation strain and microstructure. A future study will explore the effects of process scaling on sheet dimensional attributes and consistency of sheet microstructure. Work is already underway to produce larger scale 0.5 mm thick strips, initially 50 mm wide and then to 150 mm wide, to demonstrate the scalability of the HCE process.

The capability of the hybrid cutting-extrusion to produce strip in a single step even without workpiece preheating, while imposing large strains, is due to three key attributes of the deformation geometry. First, the deformation is highly confined in the process zone, see region AB in Fig. 1. As a result, there is significant adiabatic heating of the work material as it is transformed into the strip, and this heating arising from the plastic deformation-induced dissipation [7]. This is to be contrasted with the much broader deformation zone in rolling [23]. Second, the hydrostatic pressure (p) in the deformation zone is quite large, ~$2k$, where k is the shear yield stress of the material. This pressure is again significantly greater than in the rolling deformation zone (p~k). Both of these attributes of the deformation geometry are known to enhance the workability, locally, see for example Refs. [23,24]. The confinement of the deformation also has the attractive feature of reducing the deformation forces and energy, since the transformation of the work material to the strip is done incrementally (locally), as in shear spinning [29] and incremental forming processes [30]. Third, as has been recently demonstrated, the use of the constraining die can minimize or suppress shear banding [9,25], a phenomenon with adverse consequences for workability, especially in the context of sheet making. Based on the present results from AA6013-T6, and the prior work with Mg, Ti, and Fe-Si alloys, it is clear that these deformation geometry attributes of the HCE enhance the local workability of the metal, irrespective of the origins of the low workability (e.g., inadequate slip systems, microstructure, shear banding, segmentation). Also, since the constraint λ controls the deformation path (shear plane orientation), a range of shear textures, favorable for formability, can be produced in the sheet.

There are several macroscopic features of the cutting-extrusion that are worthy of mention. First, the strip in the present study was produced at speeds >1 m/s. Although commercial finish cold-rolling speeds are typically ~10 times higher in the final pass, HCE produces the strip in a single step of deformation, as against a series of deformation steps typical of conventional rolling. As a result, the overall sheet production rate for HCE is comparable to that for commercial rolling. Consequently, production rate is not a major limitation. Second, the effect of the extrusion feature, via the constraining die, enables smooth surfaces to be created on both sides of the strip, in contrast to free machining. Indeed, surface roughness measurements on the AA6013 strips show directly the effect of the constraining tool in smoothing out the roughness that naturally develops on this surface, if unconstrained as in FM (Fig. 8). The S_a value on both surfaces of the HCE strips was ~0.4 μm, very similar to that of cold-rolled sheet [28].

The HCE and FM processes could both impart large effective strains, 1 to 2, at ambient temperature, in the AA6013-T6. Such large strains are typically not possible in cold rolling of high-strength alloys, even in multiple steps, without failure by cracking. Furthermore, shear banding often occurs in rolling of higher-strength alloys. But this was not observed in the HCE of AA6013-T6, likely due to the role of the constraint in suppressing the shear band sliding phase, similar to Ti and Mg alloys [9].

The results also suggest an additional strengthening route via strain-hardening, beyond the conventional age-hardening, utilizing the cutting deformation. It is known that small amounts of strain-hardening can be imparted to age-hardened aluminum alloys by stretching, as in straightening and stress relief. However, further strengthening of age-hardened alloys by large-strain deformation is not practiced, simply for reasons of low workability. Since HCE can overcome this limitation, it allows for strain-hardening to be considered as a means of additional strengthening over and above the age-hardening, opening new possibilities for use of the corresponding T8 tempers. Although the trade-off in ductility would be an important consideration in utilizing this strengthening approach, it is instructive to consider the level of strengthening that could be achieved. The highest degree of strain-hardening achieved was for FM at ambient temperature ($\varepsilon = 1.9$, 176 HV), corresponding to a strength increase of ~30% over the base age-hardened alloy strength (Table 1). In terms of tensile strength, this corresponds to a strength change from 405 to 480 MPa. Note that a similar level of additional strengthening could also be achieved by HCE, while maintaining both sheet surfaces smooth, at a λ of 0.8.

Perhaps the most important implication of the present study pertains to HCE conducted at elevated temperatures. By preheating above a certain temperature, it was possible to produce continuous strip, in a fully dynamically recrystallized condition with equiaxed ~20 μm grains, in a single-step (Figs. 9(*a*) and 9(*b*)). In commercial rolling of 6xxx aluminum alloys, dynamic recrystallization occurs in the first stage, reversing hot-rolling process (entrance temperature 500–600 °C) [31], with a nearly equiaxed grain structure developing. However, in the subsequent, multi-stand finish hot rolling (entrance temperature 400–500 °C), dynamic recrystallization is suppressed due to the lower deformation temperature and second phase particles, resulting in a highly elongated grain structure [32,33]. In contrast, HCE of the AA6013-T6 produced dynamic recrystallization at a lower entrance temperature, $T_0 = 400$ °C, due to the higher strain and adiabatic heating compared to rolling.

The fact that static annealing of the HCE strip produced at room temperature resulted in the same recrystallized grain size (Fig. 10) as in the dynamically recrystallized samples (about 20 μm), produced with the same effective strain, strongly suggests that effective strain is the deciding factor in determining grain size. Despite similar effective strains, the flow patterns for the two cases are different, as revealed by the second-phase particle alignment (Figs. 9(*a*), 9(*b*), and 10). This indicates different strain paths possibly due to changes in flow stress and, perhaps even friction, with temperature.

The occurrence of dynamic recrystallization in the HCE has another interesting implication, in the context of heat treating the sheet back to age-hardened (T6) condition. In commercial rolling, the sheet is continuously annealed and quenched after cold-rolling to develop the solution-treated condition. However, it appears that

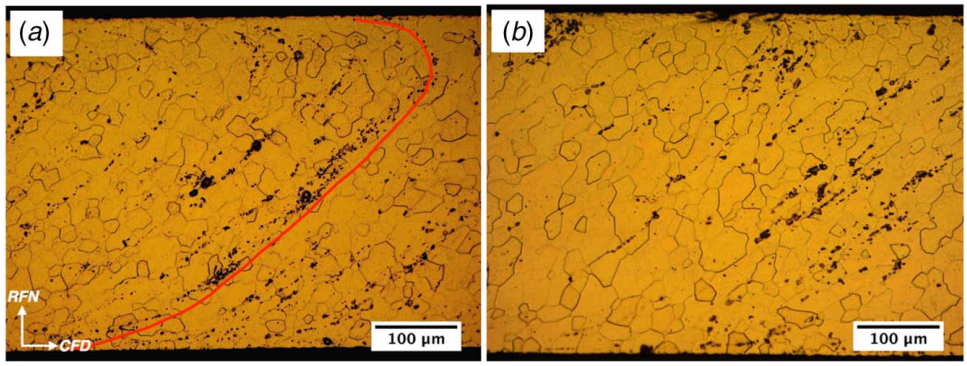

Fig. 10 Through-thickness microstructure of HCE strip statically annealed at 572 °C for 1 min: (*a*) fine-grain and (*b*) coarse-grain side. The line in (*a*) outlines the shear flow pattern.

HCE at sufficiently high temperature can yield sheet in the annealed and solution-treated condition directly. There is clear support for this in the strip produced at the lower preheat temperatures ($T_0 =$ 300 and 135 °C) after longer cooling times from above the solvus, where a lower strip hardness indicates less retained solutionization, compared to the strip produced at $T_0 = 400$ °C (Table 1). With thicker sheets, this may require the addition of a spray-quenching step; but the overall implication is that the separate annealing for solution treatment as in cold rolling would not be necessary. This type of processing is analogous to so-called, press-quenching practice in extrusion of 6xxx alloys, wherein quenching of the extrudate at the die exit produces the solutionized condition directly, without the need for a separate annealing treatment.

The primary deformation flow patterns (see Figs. 4, 6, and 7) show that both the cutting processes produce characteristic shear textures in the bulk of the strip, that are distinctly different from the texture in rolled sheet. This type of texture is indicated by the occurrence of the shear flow line type structures, with varying inclination of these flow lines to the sheet surface. This angle is controllable over a range of as much as 40 deg by varying λ and the tool rake angle; this has also been demonstrated elsewhere for Mg alloys [7]. The flow patterns are clearly demarcated also by the grain and second phase particle alignment in the structure, even at high temperatures where dynamic recrystallization occurs. Closer to the strip surfaces, however, secondary shear with flow lines oriented more parallel to these surfaces, and arising from friction with the tool surface, predominates. The contribution of this secondary shear to the sheet deformation and texture will decrease progressively with increasing strip thickness. More detailed EBSD investigation of the shear texture is currently in progress.

The shear-textured, HCE sheet has interesting implications for sheet properties, including workability. A detailed discussion of this aspect is beyond the scope of this paper but one important preliminary finding is that the highly strain-hardened HCE and FM sheet produced at ambient temperatures have exceptional cold rollability, >75%, much greater than that of conventional rolled sheet. This attribute should be of benefit for sheet metal, structural applications. Furthermore, cold rolling of the FM strip, to a reduction of even 25%, has been found to be sufficient to smooth out the surface roughness on the unconstrained face of the chip in 6013 and other aluminum alloys. This suggests the possibility also of producing sheet, directly, in a single step even by FM, followed by a light cold-rolling pass to achieve the desired surface finish.

6 Summary

A study has been made of production of sheet from high-strength, low-workability Al alloy 6013-T6 utilizing shear-based cutting and hybrid cutting-extrusion—with both processes demonstrating unique capabilities. Strips of thickness 0.2 to 0.8 mm were processed in a single deformation step, under a range of controllable thermomechanical conditions. The intense shear deformation enables processing of strips with imposed effective strains of up to 2 at ambient temperature. As a result, the strength of the age-hardened alloy was increased by up to 30%. This unusually high degree of cold-work strengthening in a high-strength, age-hardened Al alloy is typically not achievable by cold rolling due to a propensity for cracking. The capability of the cutting-based processes to produce strip in a single step, even from low-workability alloys, is likely a consequence of local enhancement in material workability in the deformation zone. This workability increase is favored by a highly confined deformation zone of intense shear, in situ plastic-deformation induced heating, and high hydrostatic pressure. Furthermore, the application of an extrusion-type constraint in the deformation zone suppresses plastic flow instabilities.

Surface topography and optical metallography characterization show the strip produced by the cutting-extrusion to have smooth surfaces on both of its sides, as low as 0.37 μm S_a. This surface quality is comparable to that of cold-rolled sheet. The strips show highly elongated grain structures (flow lines) aligned at controllable angles to the sheet faces, indicative of a shear texture. The orientation of the flow lines is determined by the shear plane angle. This shear texture is fundamentally different from the texture produced in rolling processes and may offer new opportunities for enhancing sheet formability.

Under conditions of sufficient workpiece preheating, complete dynamic recrystallization could be achieved in the strip during the cutting-extrusion. This dynamically recrystallized structure consists of fine, equiaxed grains (~20 μm), homogeneously distributed through the thickness, and independent of the starting grain size of the workpiece. The observations suggest that through controlled preheating, a homogeneous, fine-grained structure can be produced directly in alloys in a solution-treated condition. This offers the possibility of eliminating the solution-treatment annealing step, typically done before aging, in conventional production of age-hardened Al alloys.

Work is ongoing to scale up the hybrid cutting-extrusion process for larger-sized sheet, exploit its unique capability for effecting shear textures, and document benefits and disadvantages of this process vis-à-vis multistage rolling for sheet production.

Acknowledgment

Support from the National Science Foundation through Grants CMMI-1562470 and CMMI- 2100568, and the U.S. Department of Energy EERE program via Award No. DE-EE0007868 is gratefully acknowledged. We would like to thank Dr. Yiwei Sun for assistance with specimen preparation and some discussions.

AK would like to acknowledge support from the Sandia National Labs. Sandia National Laboratories is a multi-mission laboratory managed and operated by National Technology and Engineering Solutions of Sandia LLC, a wholly owned subsidiary of Honeywell

International Inc. for the U.S. Department of Energy's National Nuclear Security Administration under contract DE-NA0003525. This paper describes objective technical results and analysis. Any subjective views or opinions that might be expressed in the paper do not necessarily represent the views of the U.S. Department of Energy or the United States Government.

Conflict of Interest

There are no conflicts of interest.

Data Availability Statement

The datasets generated and supporting the findings of this article are obtainable from the corresponding author upon reasonable request. The authors attest that all data for this study are included in the paper.

References

[1] King, J. E., You, C. P., and Knott, J. F., 1981, "Serrated Yielding and the Localized Shear Failure Mode in Aluminum Alloys," Acta Metall., **29**(9), pp. 1553–1566.
[2] Kang, J., Wilkinson, D. S., Jain, M., Embury, J. D., Beaudoin, A. J., Kim, S., Mishira, R., and Sachdev, A. K., 2006, "On the Sequence of Inhomogeneous Deformation Process Occurring During Tensile Deformation of Strip Cast AA5754," Acta Mater., **54**(1), pp. 209–218.
[3] Halim, H., Wilkinson, D. S., and Niewczas, M., 2007, "The Portevin-Le Chatelier Effect and Shear Band Formation in an AA5754 Alloy," Acta Mater., **55**(12), pp. 4151–4160.
[4] Prillhofer, P., Rank, G., Berneder, J., Antrekowitsch, H., Uggowitzer, P. J., and Pogatscher, S., 2014, "Property Criteria for Automotive Al-Mg-Si Sheet Alloy," Materials., **7**(7), pp. 5047–5068.
[5] Engler, O., and Hirsch, J., 2002, "Texture Control by Thermomechanical Processing of AA6xxx Al-Mg-Si Sheet Alloys for Automotive Applications—A Review," Mater. Sci. Eng. A (1–2), **336**, pp. 249–262.
[6] Hoshi, T., and Shaw, M. C., 1977, "Cut-Forming: A New Method of Making Wire," ASME J. Eng. Ind., **99**(1), pp. 225–228.
[7] Efe, M., Moscoso, W., Trumble, K. P., Compton, W. D., and Chandrasekar, S., 2012, "Mechanics of Large Strain Extrusion Machining and Application to Deformation Processing of Magnesium Alloys," Acta Mater., **60**(5), pp. 2031–2042.
[8] Sagapuram, D., Efe, M., Moscoso, W., Chandrasekar, S., and Trumble, K. P., 2013, "Controlling Texture in Magnesium Alloy Sheet by Shear-Based Deformation Processing," Acta Mater., **61**(18), pp. 6843–6856.
[9] Sagapuram, D., Viswanathan, K., Mahato, A., Sundaram, N. K., M'Saoubi, R., Trumble, K. P., and Chandrasekar, S., 2016, "Geometric Flow Control of Shear Bands by Suppression of Viscous Sliding," Proc. R. Soc. A, **472**(2192), p. 20160167.
[10] Kustas, A. B., Sagapuram, D., Trumble, K. P., and Chandrasekar, S., 2016, "Texture Development in High-Silicon Iron Sheet Produced by Simple Shear Deformation," Metall. Mater. Trans. A, **47A**(6), pp. 3095–3108.
[11] ALCOA, Aluminum Alloy 6013, Alloy Digest, Orange, NJ, September 1987.
[12] ALCOA, Aerospace Technical Fact Sheet: Alloy 6013 Sheet, Bettendorf, IA.
[13] Issahaq, M. N., Chandrasekar, S., and Trumble, K. P., 2021, "Single-Step Shear-Based Deformation Processing of Electrical Conductor Wires," ASME J. Manuf. Sci. Eng., **143**(5), p. 051010.
[14] De Chiffre, L., 1976, "Extrusion-Cutting," Int. J. Mach. Tool Des. Res., **16**(2), pp. 137–144.
[15] Nakashima, K., Horita, Z., Nemoto, M., and Langdon, T. G., 1998, "Influence of Channel Angle on the Development of Ultrafine Grains in Equal-Channel Angular Pressing," Acta Mater., **46**(5), pp. 1589–1599.
[16] Xu, C., Furukawa, M., Horita, Z., and Langdon, T. G., 2003, "Using ECAP to Achieve Grain Refinement, Precipitate Fragmentation and High Strain Rate Superplasticity in a Spray-Cast Aluminum Alloy," Acta Mater., **51**(20), pp. 6139–6149.
[17] Hazra, S. S., Pereloma, E. V., and Gazder, A. A., 2011, "Microstructure and Mechanical Properties After Annealing of Equal-Channel Angular Pressed Interstitial-Free Steel," Acta Mater., **59**(10), pp. 4015–4029.
[18] Guo, Y., Efe, M., Moscoso, W., Sagapuram, D., Trumble, K. P., and Chandrasekar, S., 2012, "Deformation Field in Large-Strain Extrusion Machining and Implication for Deformation Processing," Scr. Mater., **66**(5), pp. 235–238.
[19] Engler, O., Tomé, C. N., and Huh, M.-Y., 2000, "A Study of Through-Thickness Texture Gradients in Rolled Sheets," Metall. Mater. Trans. A, **31A**(9), pp. 2299–2315.
[20] Mishin, O. V., Bay, B., and Jensen, J., 2000, "Through-Thickness Texture Gradients in Cold-Rolled Aluminum," Metall. Mater. Trans. A, **31A**(6), pp. 1653–1662.
[21] Truszkowski, W., Król, J., and Major, B., 1982, "On Penetration of Shear Texture Into Rolled Aluminum and Copper," Metall. Trans. A, **13A**(4), pp. 665–669.
[22] Huang, C., Murthy, T. G., Shankar, M. R., M'Saoubi, R., and Chandrasekar, S., 2008, "Temperature Rise in Severe Plastic Deformation of Titanium at Small Strain-Rates," Scr. Mater., **58**(8), pp. 663–666.
[23] Backofen, W. A., 1973, "Deformation Processing," Metall. Trans., **4**(12), pp. 2679–2699.
[24] Thomsen, E. G., Yang, C. T., and Kobayashi, S., 1965, *Mechanics of Plastic Deformation in Metal Processing*, The Macmillan Company, New York.
[25] Cai, S. L., and Dai, L. H., 2014, "Suppression of Repeated Adiabatic Shear Banding by Dynamic Large Strain Extrusion Machining," J. Mech. Phys. Solids, **73**(1), pp. 84–102.
[26] Merchant, M. E., 1945, "Mechanics of the Metal Cutting Process. I. Orthogonal Cutting and a Type 2 Chip," J. Appl. Phys., **16**(5), pp. 267–275.
[27] Townend, G. H., 1947, "Direction of Maximum Crystal Elongation During Metal Cutting," J. Appl. Phys., **18**(5), pp. 489–490.
[28] Le, H. R., and Sutcliffe, M. P. F., 2000, "Analysis of Surface Roughness of Cold-Rolled Aluminum Foil," Wear, **244**(1–2), pp. 71–78.
[29] Kalpakcioglu, S., 1961, "On the Mechanics of Shear Spinning," J. Eng. Ind., **83**(2), pp. 125–130.
[30] Jackson, K., and Allwood, J., 2009, "The Mechanics of Incremental Sheet Forming," J. Mater. Process. Technol., **209**(3), pp. 1158–1174.
[31] Totten, G. E., Funatani, K., and Xie, L., 2004, *Handbook of Metallurgical Process Design*, 2nd ed., Marcel Dekker, Inc., New York, pp. 73–74.
[32] Doherty, R. D., Hughes, D. A., Humphreys, F. J., Jonas, J. J., Jensen, D. J., Kassner, M. E., King, W. E., McNelley, T. R., McQueen, H. J., and Rollett, A. D., 1997, "Current Issues in Recrystallization: A Review," Mater. Sci. Eng. A, **238**(2), pp. 219–274.
[33] Rollett, A., Humphreys, F., Rohrer, G. S., and Hatherly, M., 2004, *Recrystallization and Related Annealing Phenomena*, 2nd ed., Elsevier, New York.